



Imager-to-radiometer
inflight cross
calibration

J. McCorkel et al.

This discussion paper is/has been under review for the journal Atmospheric Measurement Techniques (AMT). Please refer to the corresponding final paper in AMT if available.

Imager-to-radiometer inflight cross calibration: RSP radiometric comparison with airborne and satellite sensors

J. McCorkel¹, B. Cairns², and A. Wasilewski^{2,3}

¹NASA Goddard Space Flight Center, Greenbelt, MD, USA

²NASA Goddard Institute for Space Studies, New York, NY, USA

³Trinovim LLC, New York, NY, USA

Received: 9 June 2015 – Accepted: 16 September 2015 – Published: 7 October 2015

Correspondence to: J. McCorkel (joel.mccorkel@nasa.gov)

Published by Copernicus Publications on behalf of the European Geosciences Union.

Title Page

Abstract

Introduction

Conclusions

References

Tables

Figures



Back

Close

Full Screen / Esc

Printer-friendly Version

Interactive Discussion



Imager-to-radiometer inflight cross calibration

J. McCorkel et al.

Title Page

Abstract

Introduction

Conclusions

References

Tables

Figures



Back

Close

Full Screen / Esc

Printer-friendly Version

Interactive Discussion



tors and their use due to host spacecraft requirements, or the calibrator cost itself. Cost-saving strategies such as these put science results at risk of being contaminated by calibration issues such as transfer-to-orbit changes and sensor degradation while in operation. To mitigate this risk, vicarious calibration techniques can be used to transfer radiometric traceability from one sensor to another and track degradation over time.

One type of vicarious calibration that does not impose requirements on the sensor or its host spacecraft is cross-calibration with other sensors. This is common practice for researchers who need to apply a calibration to their sensor or validate that the current characterization of the sensor is stable. These activities also have the ability to identify systematic biases between sensors (Doelling et al., 2015) and promote discussion of advancing instrument design. For sensors operating in the solar reflective spectrum, most of these studies focus on comparing results of imagers, however, radiometers such as polarimeters can also benefit from these cost-saving techniques by leveraging calibration traceability from other sensors through inter-calibration.

In this work we will compare the radiometric calibration of three sensors: Research Scanning Polarimeter (RSP), Airborne Visible/Infrared Imaging Spectrometer (AVIRIS), and Landsat 8 Operational Land Imager (OLI). RSP is an airborne radiometer that scans in the along-track direction and measures the total radiance together with the Stokes parameters Q and U in nine narrow spectral channels spread across the solar reflective spectrum (Cairns et al., 1999). As described by its name, AVIRIS is an airborne imaging spectrometer that operates in the 365–2495 nm spectral range with spectral channels of approximately 10 nm bandwidth and 10 nm sampling. To form an image, AVIRIS scans in the cross-track direction at 12 Hz over a full field of view of 34° with 677 spatial samples. RSP and AVIRIS were hosted on the ER-2 aircraft in Spring 2014 for the HySPIRI Preparatory Airborne campaign where the instruments took simultaneous measurements. One particular flight line on 31 March 2014 was contemporaneous with an OLI overpass. OLI is a pushbroom imager with a 185 km swath width measuring in nine solar reflective spectral channels of which one is panchromatic across the visible to near infrared. The multispectral channels have 30 m ground sam-

This calculation also depends on the distance between the RSP and the ground, which is shown in Fig. 3 for the measurements used in this work.

There are 152 earth-view samples collected during each RSP scan. The sample closest to nadir view geometry within each scan is selected for comparison with the other sensors. The geographic location of each RSP measurement, provided in the L1 data product, is used to find the corresponding measurement within the AVIRIS and OLI data. A 60×60 pixel area centered on the AVIRIS or OLI pixel that best matches the RSP nadir measurement location is extracted from the AVIRIS and OLI imagery for each RSP measurement. The apodization mask that emulates the RSP spatial response is multiplied by each subset extracted from the AVIRIS and OLI imagery. Summing this product and dividing by the sum of the apodization mask provides AVIRIS and OLI signals that have equivalent spatial response to RSP with nearly the same viewing geometry.

Temporal, spectral and spatial parameters have been discussed and accounted for in our calibration comparison of radiometric response. In Table 1 we provide more detail regarding the uncertainties in the knowledge of offset, radiometric gain and non-linearity of response for the RSP. The dark values for the RSP are determined using 9 views of a dark reference after a dc-restore that resets an integrator. The consequent uncertainties in the determination of this dark level caused by noise are given in digital numbers (DN) and also normalized radiance units in Table 1 in the rows labeled σ_{dark} . The RSP also has a pre-dc restore measurement that is used to track drifts in the offset within a scan. The scan period is 0.8409 s and the amount of drift is currently negligible with a worst case drift of less than 0.05 DN and typical drifts of 0.005 DN. The dark reference is located 180° from the nadir view and should therefore be fairly immune to contamination by scene radiance. However, there is always some leakage/scattering of scene light into the dark reference and near field observations of a large aperture integrating sphere provide a good upper bound on such contamination, since the solid angle subtended by the sphere is large. Scattering off blackened and baffled surfaces is largest at the shortest wavelengths which is why

**Imager-to-radiometer
inflight cross
calibration**

J. McCorkel et al.

Title Page

Abstract

Introduction

Conclusions

References

Tables

Figures



Back

Close

Full Screen / Esc

Printer-friendly Version

Interactive Discussion



the contamination of the dark reference is largest at 410 nm. Even so it is only 0.08 % of the scene radiance, causing negligible radiometric errors. The radiometric uncertainty given in Table 1 has two sources. The first is the transfer uncertainty from the NIST standard source to the secondary standard source that is used for calibration: in this case a sphere (e.g. <http://cf.gsfc.nasa.gov/docs/Error/750SlickXferUncert.html>). The second source of uncertainty is the variation in the calibration, or gain, coefficient when multiple lamp levels are being fitted. These two sources of uncertainty are considered to be independent and they are therefore added in quadrature (sum of squares). An additional uncertainty at 1880 nm is absorption by water vapor in the path through the sphere, which yields an additional uncertainty of 7 % and is the primary source of uncertainty at that wavelength. Repeatability of the determination of the calibration coefficients (~ 1 % except for the 1880 nm band) is compatible with the uncertainties given here and likely changes in instrument performance after multiple ER-2 flights. Nonlinearity in the RSP detector responses can be assessed by fitting an equation of the form $RSP_intensity = a \times Lamp_Radiance^b$ to data from calibrations at multiple radiance levels. Deviations of the fitting parameter, b , from unity indicate the level of nonlinearity. The last row in the table above shows that non-linearity in the RSP response is less than 0.5 % in all bands except the 1880 nm band. Since this band is sensitive to small variations in relative humidity during the course of a calibration the larger non-linearity in that case is likely to be caused by environmental variations. Given the uncertainty in the calibrated radiances it is not possible to reject the hypothesis that the RSP sensor response is linear. In Sect. 3 we show a comparison between RSP and AVIRIS over a wide dynamic range that demonstrates that the primary difference between the sensors is the radiometric gain. The next section presents assessment and results of using data that have been put on a common spatial scale to compare radiometric gain among the sensors.

Imager-to-radiometer inflight cross calibration

J. McCorkel et al.

[Title Page](#)[Abstract](#)[Introduction](#)[Conclusions](#)[References](#)[Tables](#)[Figures](#)[Back](#)[Close](#)[Full Screen / Esc](#)[Printer-friendly Version](#)[Interactive Discussion](#)

3 Results

RSP, AVIRIS and OLI data used in this work were downloaded from each sensor's respective server on 1 September 2014, and red-green-blue snapshots from the imagers is shown in Figs. 4 and 5 where the right image in Fig. 5 is a magnification in the OLI image of the area measured by RSP and AVIRIS. The red line in Fig. 4 shows the positions of the nadir RSP measurements and the associated numbers indicate the scan number for this leg. The red lines in Fig. 5 correspond to the same locations in the OLI imagery.

Ivanpah Playa is seen in the magnified image of Fig. 5 and is the long, narrow, bright feature along the eastern edge of the image. Other flight lines flown by the ER-2 on this campaign day measured this commonly used radiometric calibration test site, but not at the time of the Landsat overpass. While there was a research team taking surface reflectance and atmospheric measurements near the center of the playa as part of AVIRIS calibration activities, this work is focusing on the inter-calibration performance between the RSP and the airborne and satellite imagers. We therefore use coincident measurements of the three sensors: the AVIRIS and RSP data used here was collected 18:13–18:17 UTC and the Landsat overpass was at 18:16 UTC on 31 March 2014.

There are 336 discrete measurement locations along the red line that is overlaid on Figs. 4 and 5. As described in the previous section, the modeled spatial response of RSP is convolved with the AVIRIS and OLI imagery to obtain signals that are spatially-equivalent signal to the RSP spatial response. These calculated signals are shown in Fig. 6 for the near-infrared channel of the sensors: OLI channel 5 and RSP channel 5. The spectral response data of RSP channel 5 was used to band-average the AVIRIS signal for this plot. The agreement in shape and fluctuations in these lines (correlation of 0.998) indicate high quality geolocation of the sensors as well as similar calibration performance. Another measure of agreement between the sensors is the similarity of the variability in each sample as shown in Fig. 7, although only AVIRIS and OLI can be gauged in this manner since each RSP measurement is a single nadir value.

AMTD

8, 10361–10386, 2015

Imager-to-radiometer inflight cross calibration

J. McCorkel et al.

Title Page

Abstract

Introduction

Conclusions

References

Tables

Figures



Back

Close

Full Screen / Esc

Printer-friendly Version

Interactive Discussion



include frequent revisit period and accurate radiometric calibration (Xiong and Barnes, 2006; Xiong et al., 2014).

As science questions grow and the availability of science funding environment becomes more limited, instrument concepts need to be developed that provide the most benefit for the least amount of cost and risk. One way to reduce cost of building an instrument is to forgo onboard calibrators and costly testing associated with them, and rely on cross calibration methods, such as the one developed in this work, to use the well-understood calibration of flagship sensors.

References

- Butler, J. J. and Barnes, R. A.: The use of transfer radiometers in validating the visible to shortwave infrared calibrations of radiance sources used by instruments in NASA's Earth Observing System, *Metrologia*, 40, S70–S77, doi:10.1088/0026-1394/40/1/316, 2003.
- Cairns, B., Russell, E. E., and Travis, L. D.: Research scanning polarimeter: calibration and ground-based measurements, in: SPIE's International Symposium on Optical Science, Engineering, and Instrumentation, International Society for Optics and Photonics, Denver, CO, 186–196, doi:10.1117/12.366329, 1999.
- Czapla-Myers, J., McCorkel, J., Anderson, N., Thome, K., Biggar, S., Helder, D., Aaron, D., Leigh, L., and Mishra, N.: The ground-based absolute radiometric calibration of Landsat 8 OLI, *Remote Sens.*, 7, 600–626, 2015.
- Doelling, D. R., Wu, A., Xiong, X., Scarino, B. R., Bhatt, R., Haney, C. O., Morstad, D., and Gopalan, A.: The radiometric stability and scaling of collection 6 terra-and aqua-MODIS VIS, NIR, and SWIR spectral bands, *IEEE T. Geosci. R.*, 53, 4520–4535, 2015.
- Knight, E. J. and Kvaran, G.: Landsat-8 operational land imager design, characterization and performance, *Remote Sens.*, 6, 10286–10305, 2014.
- Markham, B. L., Schafer, J. S., Wood Jr., F. M., Dabney, P. W., and Barker, J. L.: Monitoring large-aperture spherical integrating sources with a portable radiometer during satellite instrument calibration, *Metrologia*, 35, 643–648, doi:10.1088/0026-1394/35/4/72, 1998.

Imager-to-radiometer inflight cross calibration

J. McCorkel et al.

Title Page

Abstract

Introduction

Conclusions

References

Tables

Figures



Back

Close

Full Screen / Esc

Printer-friendly Version

Interactive Discussion



Imager-to-radiometer inflight cross calibration

J. McCorkel et al.

Title Page

Abstract

Introduction

Conclusions

References

Tables

Figures



Back

Close

Full Screen / Esc

Printer-friendly Version

Interactive Discussion



McCorkel, J., Thome, K., and Lockwood, R. B.: Absolute radiometric calibration of narrow-swath imaging sensors with reference to non-coincident wide-swath sensors, *IEEE T. Geosci. R.*, 51, 1309–1318, 2013.

Morfitt, R., Barsi, J., Levy, R., Markham, B., Micijevic, E., Ong, L., Scaramuzza, P., and Vanderwerff, K.: Landsat-8 Operational Land Imager (OLI) radiometric performance on-orbit, *Remote Sensing*, 7, 2208–2237, 2015.

Teillet, P. M., Markham, B. L., Barker, J. L., Storey, J. C., Irish, R. R., and Seiferth, J. C.: Landsat sensor cross-calibration using nearly coincidental matching scenes, in: *AeroSense 2000*, International Society for Optics and Photonics, 155–166, 2000.

Xiong, X. and Barnes, W.: An overview of MODIS radiometric calibration and characterization, *Adv. Atmos. Sci.*, 23, 69–79, 2006.

Xiong, X., Butler, J., Chiang, K., Efremova, B., Fulbright, J., Lei, N., McIntire, J., Oudrari, H., Sun, J. Q., Wang, Z. P., and Wu, A. S.: VIIRS on-orbit calibration methodology and performance, *J. Geophys. Res.-Atmos.*, 119, 5065–5078, doi:10.1002/2013JD020423, 2014.

Imager-to-radiometer inflight cross calibration

J. McCorkel et al.

Table 1. Uncertainties in dark reference determination, contamination of dark reference by scene radiance, radiometric gain and non-linearity in response.

Band (nm)	410	470	555	670	865	960	1590	1880	2260
σ_{dark} (DN)	0.22	0.22	0.22	0.17	0.23	0.20	0.27	0.28	0.27
σ_{dark} (Norm Rad.)	1.5E-5	1.2E-5	1.1E-5	1.0E-5	0.8E-6	1.0E-5	1.0E-5	1.0E-5	1.0E-5
Dark Cont. (%)	0.08	0.03	0.01	0.005	0.005	0.005	0.003	0.005	0.005
Radiometric Uncertainty (%)	1.6	1.3	1.2	1.1	0.9	0.9	0.8	7.0	2.8
Nonlinearity* (%)	0.3	0.2	0.2	0.4	0.4	0.2	0.2	0.7	0.5

* The natural log of the fitting parameter, b , described in the text multiplied by 100.

[Title Page](#)
[Abstract](#)
[Introduction](#)
[Conclusions](#)
[References](#)
[Tables](#)
[Figures](#)
[Back](#)
[Close](#)
[Full Screen / Esc](#)
[Printer-friendly Version](#)
[Interactive Discussion](#)


**Imager-to-radiometer
inflight cross
calibration**

J. McCorkel et al.

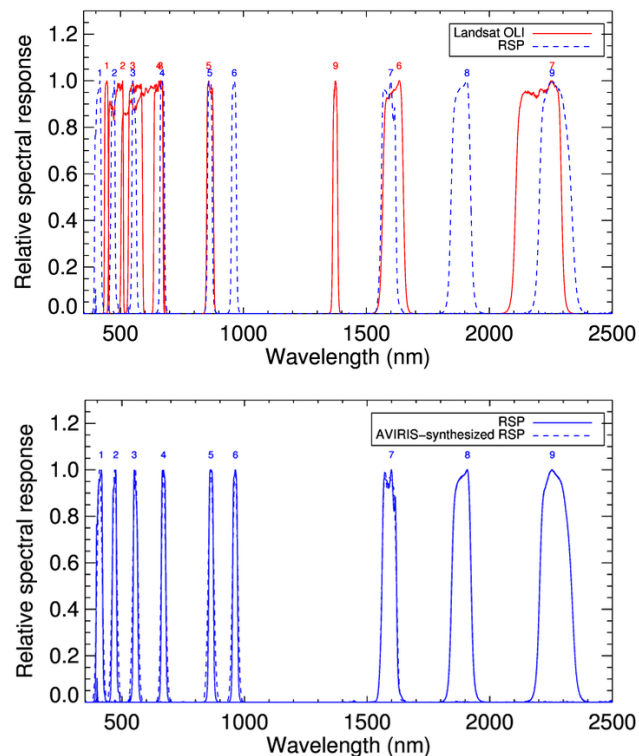


Figure 1. (a) Spectral responses of Landsat 8 OLI in solid red line and RSP in dashed blue line. (b) AVIRIS spectral channels are approximately 10 nm wide gaussian-shaped with 10 nm spacing from 365–2495 nm and weighted sums (dashed lines) have been used to match the RSP spectral channels (solid lines).

[Title Page](#)[Abstract](#)[Introduction](#)[Conclusions](#)[References](#)[Tables](#)[Figures](#)[◀](#)[▶](#)[◀](#)[▶](#)[Back](#)[Close](#)[Full Screen / Esc](#)[Printer-friendly Version](#)[Interactive Discussion](#)

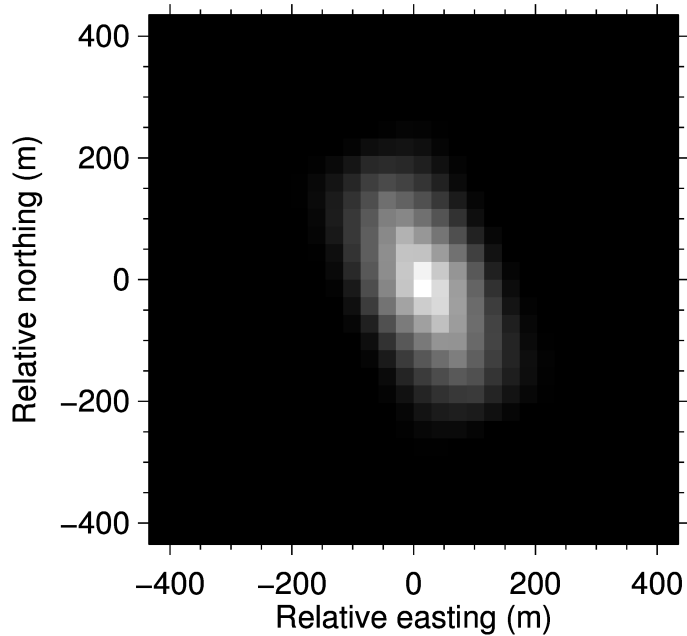


Figure 2. Modeled spatial response of a nadir RSP measurement where the long direction is along track (scan direction).

**Imager-to-radiometer
inflight cross
calibration**

J. McCorkel et al.

Title Page	
Abstract	Introduction
Conclusions	References
Tables	Figures
◀	▶
◀	▶
Back	Close
Full Screen / Esc	
Printer-friendly Version	
Interactive Discussion	



Imager-to-radiometer inflight cross calibration

J. McCorkel et al.

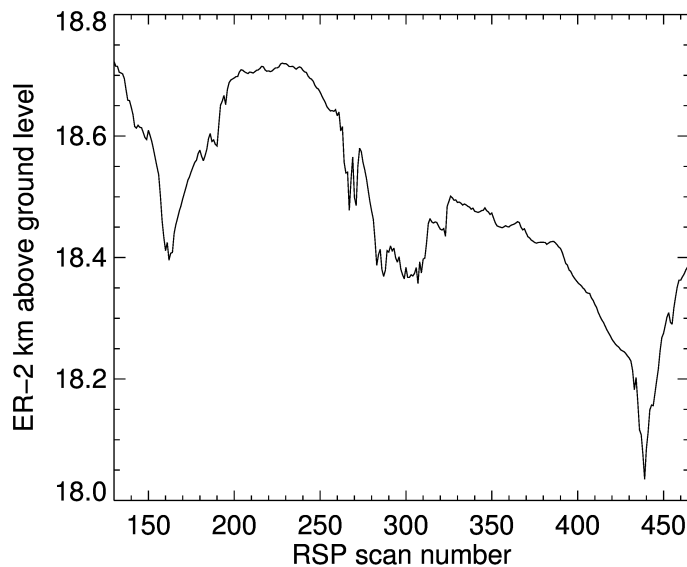


Figure 3. Although the ER-2 holds absolute altitude within tens of meters, the size of the RSP footprint will depend on the sensor’s height above ground level, which varies by almost a kilometer in the data set used here.

[Title Page](#)[Abstract](#)[Introduction](#)[Conclusions](#)[References](#)[Tables](#)[Figures](#)[Back](#)[Close](#)[Full Screen / Esc](#)[Printer-friendly Version](#)[Interactive Discussion](#)

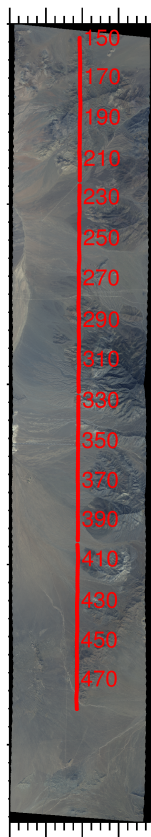


Figure 4. This image shows AVIRIS data acquired 31 March 2014 18:13–18:17 UTC in California near the southwestern California-Nevada border. The red line shows the location of the center of nadir RSP measurements where the numbers indicate the scan number.

**Imager-to-radiometer
inflight cross
calibration**

J. McCorkel et al.

Title Page

Abstract Introduction

Conclusions References

Tables Figures

◀ ▶

◀ ▶

Back Close

Full Screen / Esc

Printer-friendly Version

Interactive Discussion



**Imager-to-radiometer
inflight cross
calibration**

J. McCorkel et al.

Title Page

Abstract

Introduction

Conclusions

References

Tables

Figures



Back

Close

Full Screen / Esc

Printer-friendly Version

Interactive Discussion

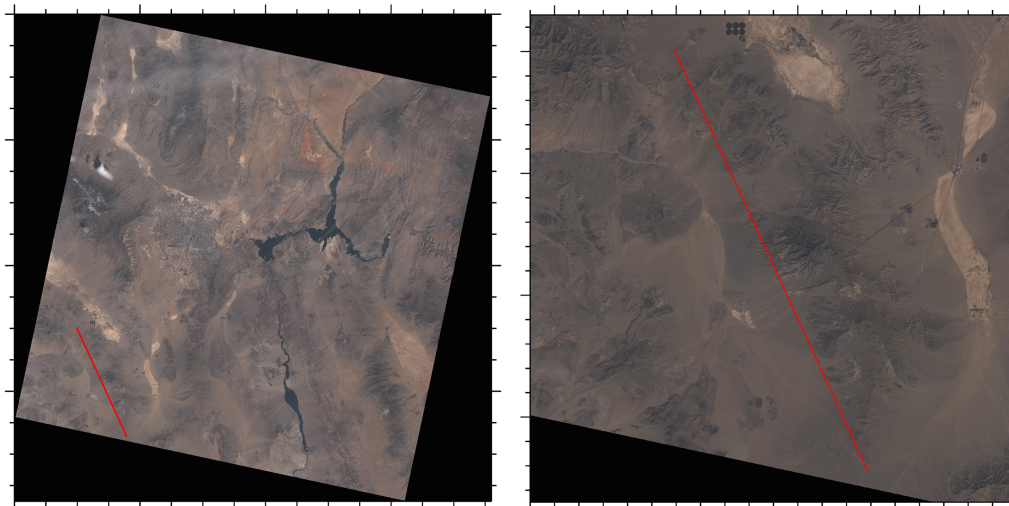


Figure 5. Landsat 8 OLI scene of southern Nevada captured on 31 March 2014 at 18:16 UTC is shown on the left. The ER-2 flight path and associated RSP and AVIRIS measurements were collected along the red line during 18:13–18:17 UTC on the same day. The flight path is 24.7° west of north with total path length of 57.1 km. The right image is a magnified view of the area of the flight line.

**Imager-to-radiometer
inflight cross
calibration**

J. McCorkel et al.

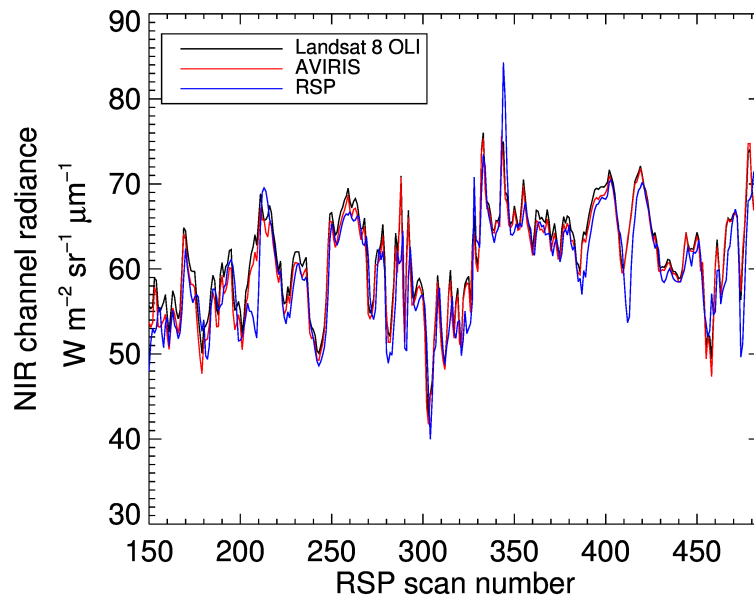


Figure 6. The signal of OLI, AVIRIS and RSP along the line formed by locations of RSP nadir measurements. The OLI and AVIRIS imagery were spatially averaged to match the RSP footprint. The AVIRIS spectrum was band-averaged to match RSP channel 5.

[Title Page](#)[Abstract](#)[Introduction](#)[Conclusions](#)[References](#)[Tables](#)[Figures](#)[◀](#)[▶](#)[◀](#)[▶](#)[Back](#)[Close](#)[Full Screen / Esc](#)[Printer-friendly Version](#)[Interactive Discussion](#)

Imager-to-radiometer inflight cross calibration

J. McCorkel et al.

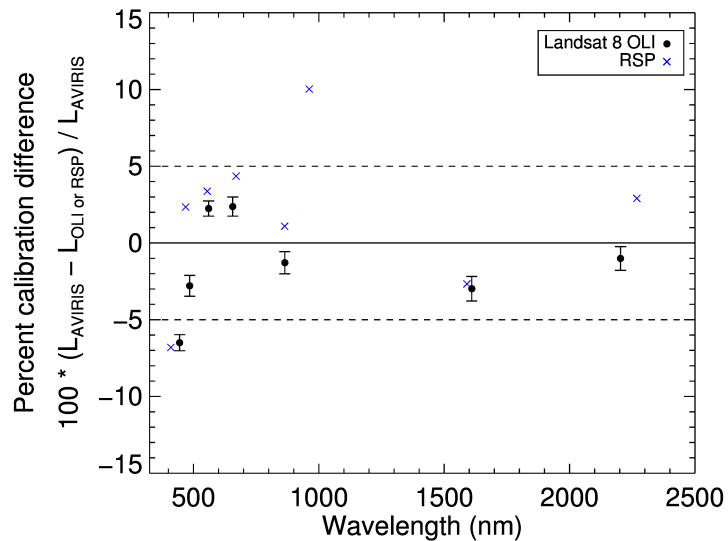


Figure 8. The percent difference in radiance between band-averaged AVIRIS and the multi-spectral sensors, RSP and OLI.

Title Page

Abstract

Introduction

Conclusions

References

Tables

Figures



Back

Close

Full Screen / Esc

Printer-friendly Version

Interactive Discussion



**Imager-to-radiometer
inflight cross
calibration**

J. McCorkel et al.

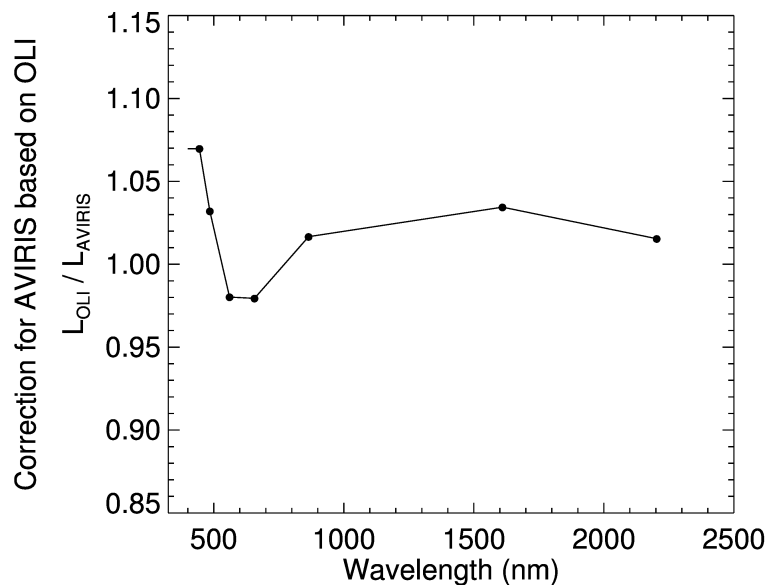
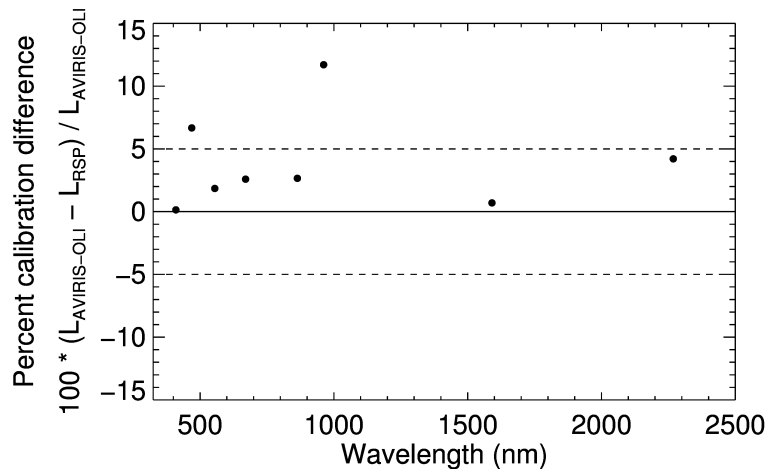


Figure 9. The ratio difference in spectral radiance between OLI and AVIRIS is used to calculate a correction curve. The multispectral points (circles) are interpolated to the spectral location of each AVIRIS channel (shown as line).

[Title Page](#)[Abstract](#)[Introduction](#)[Conclusions](#)[References](#)[Tables](#)[Figures](#)[◀](#)[▶](#)[◀](#)[▶](#)[Back](#)[Close](#)[Full Screen / Esc](#)[Printer-friendly Version](#)[Interactive Discussion](#)

**Imager-to-radiometer
inflight cross
calibration**

J. McCorkel et al.

**Figure 10.** Percent difference between RSP and OLI-calibrated AVIRIS.

Title Page

Abstract

Introduction

Conclusions

References

Tables

Figures



Back

Close

Full Screen / Esc

Printer-friendly Version

Interactive Discussion



